Environmental Science & Technology

pubs.acs.org/est

Article

Enhancing the Understanding of Soil Nitrogen Fate Using a 3D-Electrospray Sensor Roll Casted with a Thin-Layer Hydrogel

Yingzheng Fan, Xingyu Wang, Xin Qian, Anand Dixit, Brianna Herman, Yu Lei, Jeffrey McCutcheon, and Baikun Li*

Cite This: https://doi.org/10.1021/acs.est.1c05661

Read Online

ACCESS | Metrics & More | Article Recommendations | Supporting Information

ABSTRACT: Accurate and continuous monitoring of soil nitrogen is critical for determining its fate and providing early warning for swift soil nutrient management. However, the accuracy of existing electrochemical sensors is hurdled by the immobility of targeted ions, ion adsorption to soil particles, and sensor reading noise and drifting over time. In this study, polyacrylamide hydrogel with a thickness of 0.45 μm was coated on the surface of solid-state ion-selective membrane (S-ISM) sensors to absorb water contained in soil and, consequently, enhance the accuracy (R^2 > 0.98) and stability (drifting < 0.3 mV/h) of these sensors monitoring ammonium (NH_4^+) and nitrate (NO_3^-) ions in soil. An ion transport model was built to simulate the long-term NH_4^+ dynamic process (R^2 > 0.7) by considering the soil adsorption process and soil complexity. Furthermore, a soil-based denoising data processing algorithm (S-DDPA) was developed based on the unique features of soil sensors including the nonlinear mass transfer and ion diffusion on the heterogeneous sensor−hydrogel−soil interface. The 14 day tests using real-world soil demonstrated the effectiveness of S-DDPA to eliminate false signals and retrieve the actual soil nitrogen information for accurate (error: <2 mg/L) and continuous monitoring.

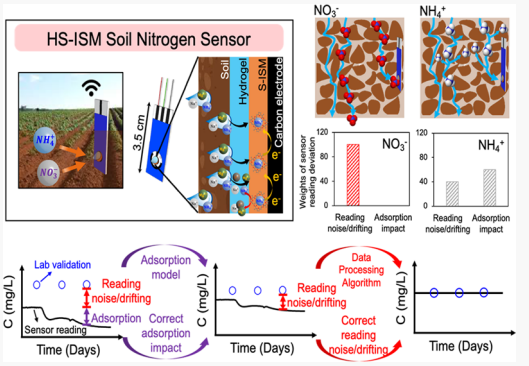

KEYWORDS: *solid-state ion-selective membrane sensors, polyacrylamide hydrogel, soil nitrogen fate, continuous monitoring, 3D electrospray, soil-based denoising data processing algorithm*

1. INTRODUCTION

As two dominant inorganic forms in the nitrogen cycle, ammonium (NH_4^+) and nitrate (NO_3^-) play a key role in plant growth and soil health.[1,2] However, soil nitrogen management is considerably difficult, since NH_4^+ is adsorbed to soil particles (negatively charged) and soil organic matters (SOM), hindering accurate measurement of NH_4^+ in soil,[3] while NO_3^- is barely attached to soil particles or SOM, resulting in the leaching to groundwater and contamination.[4] Soil nitrogen has been measured *ex situ* using lab-based approaches [e.g., gas chromatography−mass spectrometry (GC−MS) and ultraviolet−visible (UV−vis) spectrophotometry] that require soil sample transfer, pretreatment, and extraction of nitrogen from soil samples, causing severe time delay for determining the nitrogen fate in soil.[5] Potentiometric solid-state ion-selective membrane (S-ISM) sensors can partially solve these problems by real-time *in situ* monitoring nitrogen content due to their miniature dimension (electrode diameter: 2−10 mm), fast response (2−10 s), and high sensitivity (~55 mV/dec) to the analyte.[6] S-ISM sensors (e.g., carbon-nanotube solid-state NH_4^+ sensors,[7] NO_3^- poly(tetrafluoroethylene) (PTFE)-loaded sensors,[8] polypyrrole PPy(NO_3^-),[9] and molybdenum disulfide (MoS2)−poly(3-octyl-thiophene)[10] sensors) have been developed for *in situ* monitoring of nitrogen species in water and wastewater based on the equilibrium concentration of the targeted ions between the surface of sensor membrane and the water solution. However, S-ISM sensors cannot be used in soil, since the hydrophobic sensor surface [e.g., poly(vinyl chloride) (PVC)[11]] tends to hinder water from attaching onto the sensor surface, thus restricting the continuous mobility of the targeted ions into the sensor polymer matrix.

Previous efforts have enhanced hydrophilicity of the sensor surface (e.g., coating a hydrophilic SiOx film onto the Pt electrode, fabricating a hydrophilic SiO_2/Si diaphragm sensor).[12,13] However, these sensors suffer from severe reading declination when the volumetric soil water content (%) drops below 15%,[12,13] since these hydrophilic sensor surfaces can only prevent water from moving away from the sensor surface but fail at absorbing more water from soil. These sensors cannot, therefore, facilitate the transport of targeted ions from the soil toward the sensor surface. Hydrogel can be a feasible solution for

Received: August 23, 2021
Revised: February 24, 2022
Accepted: February 25, 2022

such a problem due to its highly cross-linking water-absorbent polymeric networks.[14] Various types of hydrogels (e.g., nanocomposite hydrogels, chitosan hydrogels, and carboxymethyl cellulose-based hydrogel) have been used for oil recovery,[15] water treatment,[16] and human tissue augmentation,[17] but for sensor applications, hydrogel has been limited to human wearable sensors targeting human pressure,[18] glucose,[19] and serum.[20] Furthermore, although existing hydrogel-coating methods (e.g., surface bridge method,[21] surface initiation method,[22] and paint method[23]) enable a strong adhesion of hydrogel onto the substratum sensor surface, these methods fail at creating ultrathin films (<3 μm) required for proper operation of soil S-ISM sensors.

Long-term continuous monitoring of nitrogen species in soil using S-ISM sensors has the potential to provide real-time information necessary for determining the nitrogen fate in soil and managing soil nutrients. However, in terms of NH_4^+ monitoring, it is challenging to validate its dynamic process due to the complex adsorption process. Many studies used chemical equilibrium models (e.g., local equilibrium during ammonium transport, leaching prediction model)[24,25] containing the fixed retardation factors to simulate a short-term (e.g., hours) NH_4^+ dynamic process, but these models would substantially deviate from the real-world scenario for the long-term process (at the scale of days or months) due to the time-varying adsorption rate,[26] hindering accurate compensation of NH_4^+ sensor reading deviations. In contrast, there is a minimal exchange between NO_3^- and negatively charged soil particles, in which the adsorption impact would not be considered for NO_3^- monitoring.[27] Additionally, during the long-term monitoring process, soil sensor accuracy could deteriorate due to sensor reading noise (fluctuation of sensor readings around the real values) and sensor reading drifting (stray of sensor readings from the real values). Diverse sensor materials (e.g., polymers,[11] nanoparticles[28]) have been developed to enhance the accuracy of S-ISM sensors, but the long-term performance of these newly developed materials is still unknown. Hence, mathematical algorithms [e.g., machine learning algorithms (ML),[29] digital filters[30]] have been applied to address these noise/drifting by extracting sensor features and exceptions or embedding electrochemical models. However, ML processes data with poor interpretability in a "black box" mode and requires humongous data sets (e.g., over 3 years data[31]) to train models, and digital filters cannot percolate anomalies from the raw S-ISM sensor data due to the continuously varying sensor readings. Recently, water-based denoising data processing algorithm (W-DDPA) was developed to differentiate noise using Taylor series.[32] However, such water-based models cannot fit for soil S-ISM sensors due to the distinct difference between soil properties and water properties, as well as the drastic difference of the nitrogen diffusion process between the water–sensor interface and the soil–hydrogel–sensor interface. Therefore, soil sensor readings suffer from false noise intensity when W-DDPA is directly applied to process the readings.

The rationale of this study lies in providing an innovative understanding of nitrogen fate in soil through real-time *in situ*, long-term and continuous monitoring of soil nitrogen species (NH_4^+ and NO_3) using hydrogel-coated S-ISM (HS-ISM) sensors. An optimal thickness of a polyacrylamide hydrogel layer is determined for the electrosprayed S-ISM sensor surface so as to absorb water contained in soil to the sensor surface, thus sustaining ion equilibrium between the sensor and soil and enhancing the accuracy, sensitivity, and stability of soil sensors. A novel ion transport model is developed to simulate the long-term NH_4^+ dynamic process by considering the varying soil adsorption process and soil complexity. A soil-based denoising data processing algorithm (S-DDPA) is developed by considering the unique features of HS-ISM soil sensors, including the nonlinear mass transfer and ion diffusion at the heterogeneous sensor–hydrogel–soil interface, to eliminate false signals and retrieve the actual soil information for precise soil nitrogen control and decision making.

2. MATERIALS AND METHODS

2.1. Fabrication of a Hydrogel-Coated S-ISM (HS-ISM) Nitrogen (NH_4^+/NO_3^-) Soil Sensor Using Electrospray and Roll-Casting Methods. The sensor support (length: 3.5 cm, width: 1.5 cm, thickness: 0.1 cm, aerial view: Figure 1a) was

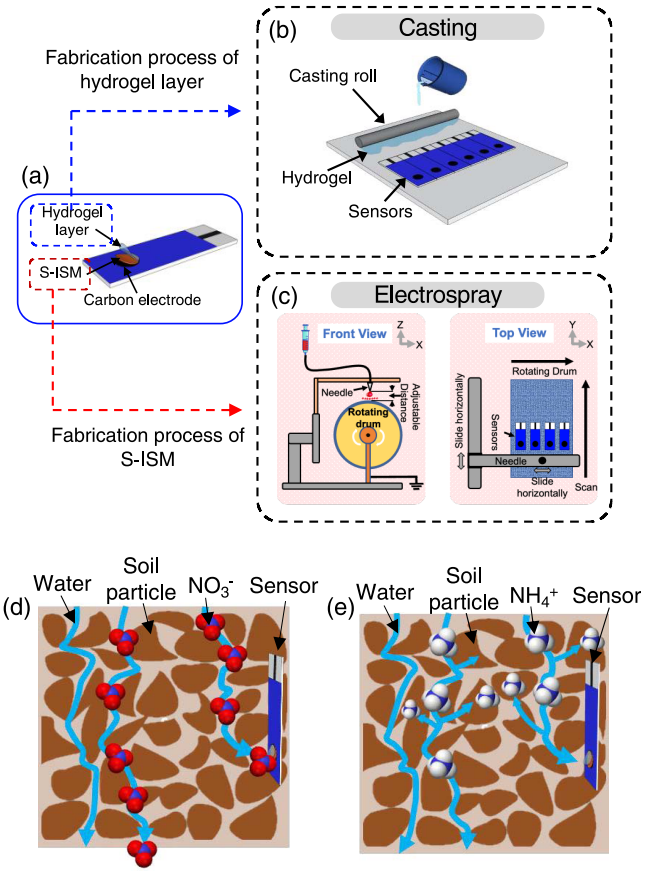

Figure 1. Fabrication process of a (a) HS-ISM nitrogen (NH_4^+/NO_3^-) soil sensor (b) using electrospray for S-ISM (c) and roll-casting methods for the hydrogel layer. The transport process of (d) NO_3^- and (e) NH_4^+ ions in soil.

fabricated by the conventional screen-printing technology (SPT). NH_4^+ and NO_3^- ion-selective membrane (ISM) cocktails were synthesized individually following the protocols reported previously,[33] but the fabrication process was further improved using three-dimensional (3D) electrospray printing technology that can effectively reduce the membrane roughness and thickness to 1 μm (Figure 1b).[34] The detailed procedure of the electrospray process is described in Text S1. The synthesis process of polyacrylamide hydrogels was improved in a previous study.[35] First, 4.3 wt % of acrylamide (AAm) (Sigma-Aldrich) powder was dissolved in 100 mL of distilled water and was stirred ~1 h to form an aqueous solution. Subsequently, *N*,*N*′-

https://doi.org/10.1021/acs.est.1c05661
Environ. Sci. Technol. XXXX, XXX, XXX−XXX

methylenebis(acrylamide) (MBAA, Sigma-Aldrich), *N*,*N*,*N*′,*N*′-tetramethylethylenediamine (TEMED, Sigma-Aldrich), and ammonium persulfate (APS, Sigma-Aldrich) in quantities of 0.06, 0.25, and 1% times the weight of AAM were sequentially added into the solution and was stirred using a magnetic stirrer at the room temperature for 10 min to form a homogeneous polyacrylamide hydrogel solution. After the synthesis, the hydrogel solution was casted using casting rods over the solid-state ISM (S-ISM) sensors attached to the clean glass plate at room temperature (Figure 1c). Finally, the hydrogel coated onto the S-ISM was dried over 24 h under a lightless environment to form HS-ISM sensors.

2.2. Characterization Analysis of HS-ISM Nitrogen Soil Sensors. The cross section of nitrogen HS-ISM sensors was observed using a scanning electron microscope (SEM) (FEI Nova NanoSEM 450) and the average thickness of the hydrogel layer was calculated using FIJI (ImageJ) software (Text S2). The electrochemical impedance spectroscopy (EIS) was conducted in 0.1 M KCl solution to characterize the difference between S-ISM and HS-ISM. The results were recorded in the frequency range from 100 kHz to 0.1 Hz using an excitation amplitude (ΔE_{ac}) of 10 mV, and the data was fitted based on the equivalent circuit models in ZSimpWin software. In addition, the water-absorbent property of S-ISM and HS-ISM was examined by measuring the contact angle using a CAM 101 optical surface tension meter (KSV Instrument Inc.).

Calibration and selectivity tests followed previous soil sensor studies (Text S3).[10] Briefly, the sensor reading [open-circuit potential (OCP): mV] was recorded at 0.1 s intervals using a multichannel electrochemical workstation (CHI 660D potentiostat) in the corresponding concentration of nitrogen (NH_4^+/NO_3^-) solutions (1, 4, 16, 64, and 128 mg/L). The calibration result was collected to evaluate sensor performance and sensitivity over time and then fed into a data processing algorithm to enhance the reading accuracy, as discussed in Section 3.4. The selectivity test was conducted by adding different ions, including NH_4^+, Mg^{2+}, Na^+, Al^{3+}, and Ca^{2+} for NH_4^+ HS-ISM sensors and NO_3^-, Cl^-, SO_4^{2-} and PO_4^{3-} for NO_3^- HS-ISM sensors. All of the tests were triplicated, and the average values were calculated. Besides, soil organic matters (SOM) in the soil matrix could also interfere with the selectivity of soil sensors.[36] Thereby, an interference test was conducted by adding multiple organic salt solutions (20 mL of 1 mg/L sodium acetate, 20 mL of 1 mg/L sodium oxalate, and 20 mL of 1 mg/L sodium lactate) simultaneously into the soil (~85 g) to simulate the SOM variation in soil. The SOM content (%) in soil was measured using the Walkley−Black method (Text S4). However, the added organic salts might be adsorbed to soil particles and not available in the porewater, which might underestimate the interference of organic salts for our soil sensors. To avoid such possibility, the HS-ISM soil nitrogen sensors were also examined in the water solution (volume: 100 mL) that simulated the dissolved organic carbon (DOC) in the porewater of soil particles. Specifically, multiple organic salt solutions (5 μL of 1 mg/L sodium acetate, 5 μL of 1 mg/L sodium oxalate, and 5 μL of 1 mg/L sodium lactate) were simultaneously added into the water solution (volume: 100 mL). The readings (mV) of nitrogen (NH_4^+/NO_3^-) HS-ISM soil sensors before and after the addition of organic salts were recorded using an EmStat blue wireless potentiostat.

2.3. Long-Term Continuous Monitoring of HS-ISM Nitrogen Sensors in Real-World Soil. The long-term performance of NH_4^+ and NO_3^- HS-ISM nitrogen sensors was examined by inserting these two types of sensors into soils for 14 days. To best resemble the real-world field test environment, the soil samples were taken from the Plant Science Research and Education Facility at the University of Connecticut, Storrs, CT, with a bulk soil density of 1.93 g/mL and 78% of the soil particle diameters less than 1.00 mm. The soil we used was a Woodbridge fine sandy loam soil (a coarse-loamy, isotic, mesic Aquic Humudepts), and the detailed characteristics of the soil are described in Table S1. Soil was homogenized by picking out small rocks and smashing the clotted soil blocks. Then, these soil samples (~85 g) were firmly compacted into a plastic beaker (diameter: 4 cm, height: 5 cm), so that the HS-ISM sensors could be firmly inserted into the soil at a depth of 2 cm (Figure S1). During the 14 day test period, two shocks of 20 mL of the concentrated solution (30 and 60 mg/L for NO_3^-, 15 and 15 mg/L for NH_4^+) were added individually into the soil beaker on the second day and eighth day to examine the accuracy of nitrogen soil sensors under drastic variation of nitrogen concentration. Around 0.5 g of the soil sample was taken from the soil beaker once per 2 days to measure the volumetric water content (%) by weighing these soil samples before and after oven-drying for 24 h at 105 °C. The OCP readings (mV) of both NH_4^+ and NO_3^- HS-ISM sensors were continuously recorded at an interval of 30 s using an EmStat blue wireless potentiostat, so that all of the sensor data could be collected remotely in a real-time mode. All of the long-term continuous measurements were triplicated, and the average values were calculated. Throughout the test period, the conventional 2.0 M KCl extraction (Text S3) method was used to extract the soluble and absorbed nitrogen in soil. The validation result (mg/L) was converted by the extraction method based on extraction solution volume and soil bulk density.

2.4. Model Development for the Ammonium Transport Process. To quantify the influence of NH_4^+ adsorption on the sensor accuracy during long-term monitoring (Figure 1d,e), a transport model was developed to simulate NH_4^+ sensor readings, as described in the convection−dispersion equation (eq 1)[37]

$$\frac{\partial C\ (z,\ t)}{\partial t} = -\frac{v}{R}\frac{\partial C\ (z,\ t)}{\partial z} + \frac{D_L}{R}\frac{\partial^2 C\ (z,\ t)}{\partial z^2} \tag{1}$$

where $C\ (z,t)$ is the NH_4^+ concentration in soil, z (cm) is the depth of the soil/distance from the soil surface, t (day) is time, v is the seepage velocity, D_L is the dispersion coefficient, and R is the retardation factor. In this model, R was ascribed to the chemical adsorption of NH_4^+ to soil particles, which gradually reaches the equilibrium as a kinetic behavior and thus correlating with the time-dependent partition coefficient ($\frac{\partial K_d}{\partial t}$) (eq 2)[26]

$$\frac{\partial K_d}{\partial t} = \alpha[(1 - F)K_L C - K_d] \tag{2}$$

where α is the first-order rate coefficient, F is the fraction of adsorption sites, and K_L is the linear adsorption coefficient. Soil complexity, including hydraulic conductivity (K), effective porosity (θ_e), effective saturation (S_e), and wetting from soil suction head (Ψ), was determined for seepage velocity (eq 3)[38]

$$v(t) = K\left(\frac{\Psi\theta_e(1 - S_e)}{K_t + \Psi\theta_e(1 - S_e)\left(1 + \frac{V(t)}{\Psi\theta_e(1 - S_e)}\right)} + 1\right) \tag{3}$$

https://doi.org/10.1021/acs.est.1c05661
Environ. Sci. Technol. XXXX, XXX, XXX−XXX

The boundary condition was the initial concentration (M_i) at the initial state ($t = 0$), which was pulse injected into the soil from the top layer ($z = 0$). To sum up, the time-dependent adsorption process was applied into the simulation of the transport process to minimize the impact of NH_4^+ adsorption for soil sensor readings. Values of the parameters in this model are listed in Table S2. More details of this model are described in Text S5.

2.5. S-DDPA Algorithms for Data Processing in Soil over the Long-Term Monitoring Period. The HS-ISM soil sensors require an adaptable processing algorithm to correct their reading noise and drifting. In line with the nitrogen mass transfer through soil particles, hydrogel diffusion, and adsorption dynamic process on the soil−hydrogel−sensor interface, a novel soil-based DDPA (S-DDPA) was developed from the water-based DDPA (W-DDPA) previously developed[32] by adding a double median filter, the Langmuir adsorption model, and the nonequilibrium mass transfer model to eliminate the sensor signal noise and adjust the reading drifting in soil.[32] Furthermore, the S-DDPA incorporated the Nernst slope alternation (once per 2 days) to compensate the fixed slope limit of the W-DDPA (eq 4)

$$f(t) = \frac{K_{eq}p}{1 + K_{eq}p}\left(\sum_{i=0}^{n} f(t)L_i(t) + \frac{f(n+1)(\xi)}{(n+1)!}\left(\prod_{i=0}^{n}(t - t_i)\right)\right)$$

$$\xi \in (\min(x_0, x_1, \cdots, x_n), \max(x_0, x_1, \cdots, x_n)) \quad (4)$$

where K_{eq} is the adsorption equilibrium constant, p is the partial pressure of the target ions (NH_4^+/NO_3^-), n represents the order of differentiation with the upper limit of 10 in this study, and t is time. $L_i(t)$ is a Lagrange polynomial representing a Kronecker data (eq 5)

$$L_i(t) = \prod_{m \neq j} \frac{x_i - x_m}{x_j - x_m} = \delta_{ij} = \begin{cases} 0 & \text{if } i = j \\ 1 & \text{if } i \neq j \end{cases} \quad (5)$$

The original data set and approximated derivative properties were analyzed through the density-based method. The distribution of these data was expressed as a distance-based probability density entropy (eq 6)

$$E = -\sum_{i}^{m} [p_i \log(p_i) + (1 - p_i)\log(1 - p_i)] \quad (6)$$

This equation decomposed sensor signals into different levels of derivatives, deeply analyzed the distribution of the sensor OCP data, distinguished all possible abnormalities out of Nernst response, and precisely filtered out the noise to achieve a stable and accurate output of HS-ISM sensors in soil.

3. RESULTS AND DISCUSSION

3.1. Enhancement of Water-Absorbent Property and Determination of the Optimal Thickness of the Polyacrylamide Hydrogel Layer. HS-ISM nitrogen (NH_4^+/NO_3^-) soil sensors rely on the roll-casted polyacrylamide hydrogel layer coated onto the surface of the electrosprayed nitrogen solid-state ion-selective membrane. The SEM and energy-dispersive X-ray spectroscopy (EDS) images of the cross-sectional morphology of the HS-ISM nitrogen soil sensor clearly displayed a three-layer structure, including hydrogel layer, S-ISM matrix, and carbon electrode (Figure 2a). The presence of oxygen (O) and nitrogen (N) elements in the first layer in the EDS images indicated the polyacrylamide hydrogel coating onto the surface of the ISM (Figures 2a and S2a), while chloride (Cl) and titanium (Ti) in the EDS images represented S-ISM and a carbon electrode (Figures 2a and S2b). Here, the

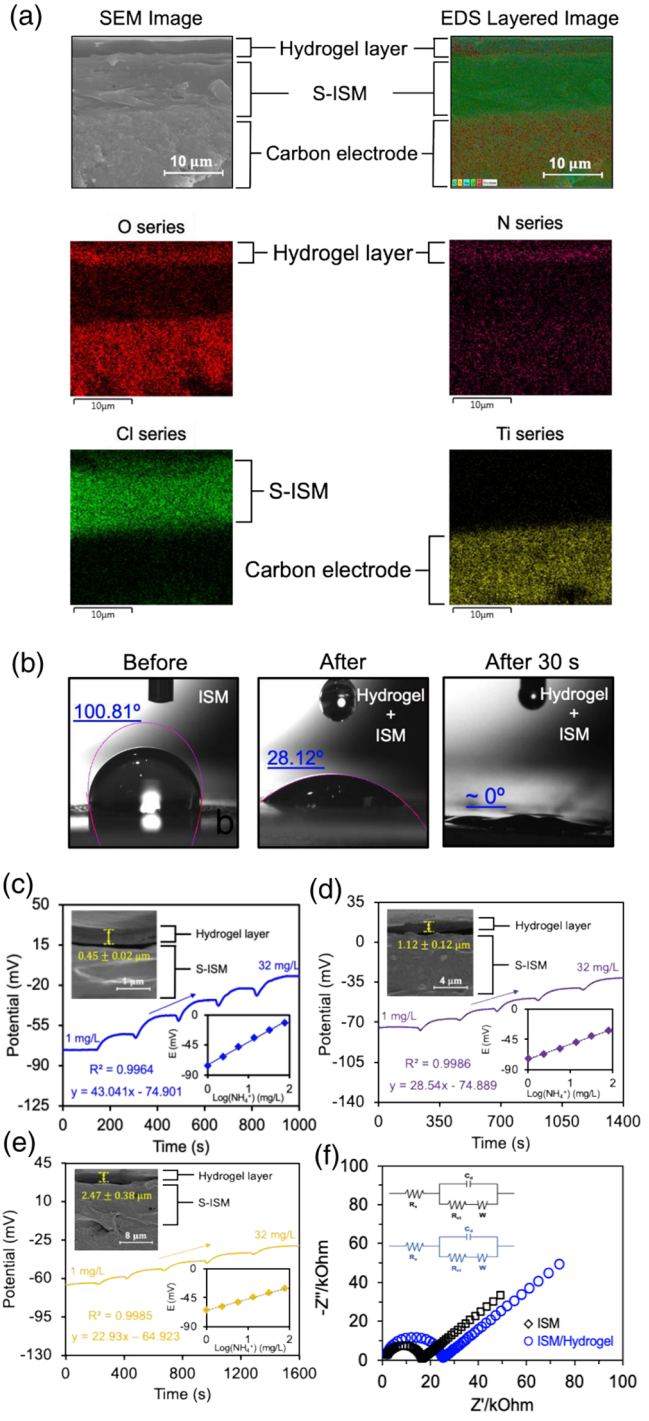

Figure 2. (a) SEM and EDS images of the cross section of an HS-ISM sensor. (b) Images and outlines of the water-contact angle at surfaces of S-ISM, HS-ISM, and 30s-latent HS-ISM. Calibration curves of an HS-ISM sensor with different hydrogel thicknesses [(c) 0.45, (d) 1.12, (e) 2.47 μm]. (f) Impedance analysis of S-ISM and HS-ISM sensors (The inset schematics depict the corresponding equivalent circuit diagram models.).

https://doi.org/10.1021/acs.est.1c05661
Environ. Sci. Technol. XXXX, XXX, XXX−XXX

polyacrylamide hydrogel as the water-absorbent layer continuously sustains the ion equilibrium on the sensor surface in the soil environment. The water-absorbent property was attributed to the contained water solubility groups such as $-NH_2$ and $-CONH_2$ in the chemical structure of the polyacrylamide hydrogel (Figure S3). Compared with the traditional hydrophobic nitrogen S-ISM sensor surface (100.81°, Figure 2b), the water-contact angle of this hydrogel-coated sensor surface was only ~28° (Figure 2b), indicating tremendous enhancement of the hydrophilicity of the hydrogel-coated sensor surface. In addition, after a water droplet was dropped onto the hydrogel-coated sensor surface for around 30 s, the water-contact angle becomes ~0° (Figure 2b), proving the unique water-absorbent property of this polyacrylamide hydrogel layer.

To determine the optimal polyacrylamide hydrogel thickness, HS-ISM sensors with three hydrogel thicknesses (0.45 ± 0.02, 1.12 ± 0.12, and 2.47 ± 0.38 μm, Figure 2c–e, inset images) were examined in nitrogen solutions ranging from 1 to 32 mg/L. Here, 0.45 μm was the minimum thickness to form an integrated layer of the hydrogel and fully cover the S-ISM surface, while the sensor response became much slow (>150 s) when hydrogel thickness increased to 2.47 μm, which cannot meet the requirement of *in situ* soil monitoring and might cause confusion for sensor data collection and interpretation in the field. Hence, the thickest hydrogel layer was set as 2.47 μm in this study. Among these three different thicknesses, the HS-ISM sensor with the thinnest hydrogel layer (0.45 ± 0.02 μm) displayed the highest Nernstian slope of 43.04 mV/dec (the theoretical Nernstian slope for monovalent ions (e.g., NH_4^+ and NO_3^-): 59 mV/dec) and the fastest response (<50 s), which was verified by the principle of permeability (P) across the hydrogel membrane layer. Permeability is a measure of the easiness of an ion crossing the membrane (eq 7)[39,40]

$$P = \frac{KD}{X} \tag{7}$$

where K is the partition coefficient,[41] D is the diffusion coefficient, and X is the thickness of the hydrogel layer. The diffusion coefficient of solute (D) in the hydrogel can be calculated using the polymer volume fraction ($\varnothing$) based on the obstruction scaling theory (eq 8)[42,43]

$$D = \exp\left[-\pi\left(\frac{r_s + r_f}{k_s \alpha \varphi^{-0.75} C_\infty^{-0.25}(1 - 2\varnothing)^{-0.25} + 2r_f}\right)^2\right] \cdot D_0 \tag{8}$$

where r_s is the radius of the solute in the hydrogel, r_f is the radius of the polymer chain, α is the equivalent bond length of the monomer (acrylamide), φ is the polymer volume fraction, C_∞ is the characteristic ratio of the polymer, $\varnothing$ is the Flory–Huggins polymer interaction parameter, D_0 is the diffusion coefficient of the solute in water, and k_s is the fitting parameter. Values of these parameters are listed in Table S3. According to eqs 7 and 8, the high diffusion coefficient (1.29×10^{-5} cm/s, Table S4) of the polyacrylamide hydrogel achieved in this study was mainly attributed to the low volume (4.3% v/v) of the polymer matrix used. Notably, this diffusion coefficient was higher than the other hydrogels exported, including poly(ethylene glycol) (PEG) hydrogel (10^{-6} to 10^{-7} cm^2/s)[44] and chitosan/poly(vinyl alcohol) hydrogel (1.9×10^{-6} to 6.1×10^{-6} cm^2/s).[45] This high diffusion coefficient and the thinnest layer (0.45 ± 0.02 μm) resulted in the highest permeability (eq 7 and Table S4) of the hydrogel layer for ions to pass through, which was validated by the experimental results of the highest Nernstian slope (43.04 mV/dec) and fastest response (<50 s). Although the response time was longer than the previous S-ISM sensors without the hydrogel layer (53.48 mV/dec, <10 s)[33] due to the high membrane resistance (as shown in the EIS result, Figure 2f), this increment did not impair the hydrogel sensor's accuracy (R^2 > 0.99). In general, this polyacrylamide thinnest hydrogel layer (thickness: 0.45 ± 0.02 μm) was selected as the optimal thickness for HS-ISM sensors due to its balanced sensitivity, response, and accuracy.

3.2. Characteristics of HS-ISM Nitrogen Soil Sensors in Soil. The calibration of nitrogen (NH_4^+ and NO_3^-) HS-ISM soil sensors with the thinnest hydrogel layer was each conducted in soil under the concentration ranging from 1 to 128 mg/L, i.e., spanning the typical soil nitrogen range regulated.[46] These nitrogen HS-ISM soil sensors exhibited an excellent accuracy (R^2 = 0.98 for NH_4^+, R^2 = 0.98 for NO_3^-, Figure 3a,b), which markedly surpassed the potentiometric soil sensors previously reported (R^2 < 0.9).[47,48] This excellent accuracy was even comparable to some water nitrogen sensors, such as an enzymatic (R^2 = 0.98)[49] and polypyrrole-coated palladium nanocluster (Pd-NCs-PPy) nitrate sensor (R^2 = 0.98).[50] More importantly, various ions present in real-world soil environments pose a challenge for the selectivity of nitrogen sensors. The tests showed that the potential (mV) readings of the NH_4^+ HS-ISM soil sensor responded solely to the targeted NH_4^+ ion and remained intact after adding the interfering cations (Mg^{2+}, Na^+, Al^{3+}, and Ca^{2+}, Figure 3c). Likewise, various nontarget anions (NO_3^-, Cl^-, SO_4^{2-}, and PO_4^{3-}) caused nearly negligible interference to the readings of NO_3^- HS-ISM sensors (Figure

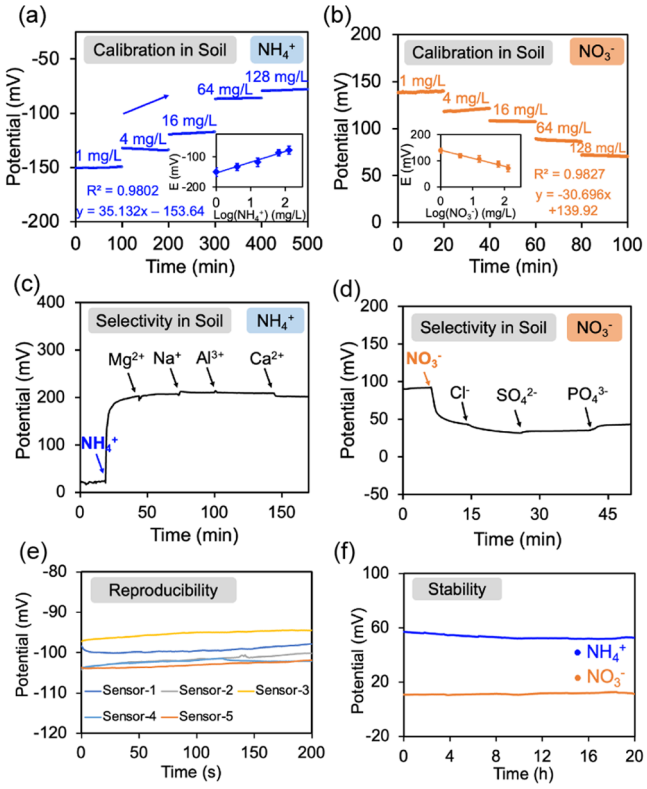

Figure 3. Calibration curve of (a) NH_4^+ and (b) NO_3^- HS-ISM sensors in soil. Selectivity tests of (c) NH_4^+ and (d) NO_3^- HS-ISM sensors in soil. (e) Reproducibility test of an HS-ISM soil sensor. (f) Stability test of an HS-ISM soil sensor.

https://doi.org/10.1021/acs.est.1c05661
Environ. Sci. Technol. XXXX, XXX, XXX–XXX

3d), indicating that the hydrogel coating did not compromise the selectivity of HS-ISM sensors. This high selectivity is mainly ascribed to the bonding receptors (hydrogen bonds for NH_4^+, NH bonds as H bond for NO_3^-) of ionophores and the cavity of ionophores only fitting for the targeted ions (ionic radii for NH_4^+: 0.143 nm, for NO_3^-: 0.179 nm).[51,52]

In addition, SOM (e.g., acetate) contained in soil particles and soil porewater can cause pH variation due to conjugation and might interfere with the soil sensor readings.[53] However, the rates for salt formation in soil suspension are as low as 35−220 μg of acetate per gram (g) of soil and cannot affect the pH of soil solution due to the negligible concertation.[54] To determine whether SOM in soil could influence HS-ISM soil sensors, low concentration (1 mg/L) of multiple organic salts (e.g., acetate, oxalate, and lactate) was added into the soil simultaneously. The readings of both NH_4^+ and NO_3^- HS-ISM sensors barely varied after adding these SOMs (Figure S4), during which the SOM concentration (%) in soil increased from 0.05 in the intrinsic soil to 0.16 after the introduction of organic salts. However, the interference tests in the soil cannot eliminate the possibility that the added organic salts might be mostly adsorbed to the soil and not available in the porewater. A parallel test in the water solution was conducted to simulate DOC in porewater. The results revealed that the HS-ISM sensors evidently responded to the target ions rather than these DOCs (Figure S5), demonstrating that neither SOM in soil nor DOC in porewater interfered with the *in situ* monitoring accuracy of HS-ISM nitrogen sensors. It should be noted that although the pH impact on the hydrogel structure was found in previous studies,[55] the pH value was kept at a stable level (~5.9) in the soil container in this study, making the pH interference negligible.

To investigate the reproducibility of HS-ISM sensors, we measured the initial potentials (E^0) of five pieces of sensors fabricated from the same batch. The E^0 values among these electrodes were quite close (−95.13 to −102.79 mV, Figure 3e), as evident by the low relative standard deviation (RSD = 3.14%), which was attributed to the controllable thickness of S-ISM (~10 μm, Figure 2a) coated using 3D electrospray and the thin hydrogel layer (~0.45 μm, Figure 2c) casted using the roll coating technique. Furthermore, the potential variation (ΔE) of these HS-ISM nitrogen sensors during a 20 h period was fairly slight with 0.3 mV/h for NH_4^+ sensors and 0.1 mV/h for NO_3^- sensors (Figure 3f), which was amazingly lower than other water sensors, such as PTFE-load nitrate S-ISM sensors (0.9 mV/h),[8] inkjet-printed nitrate S-ISM sensors (0.9 mV/h),[56] and ruthenium dioxide-based pH sensors (0.38 mV/h).[57] This superb stability resulted from a tiny amount of the S-ISM polymer solute coated onto the electrode substrate using the 3D-electrospray printing technology (Figure 1) and the deposition of the next layer carrying some excessive solvent (e.g., tetrahydrofuran) that could redissolve the previously printed layers and strengthen the affinity of S-ISM with the carbon electrode.[58]

3.3. Long-Term Continuous Real-Time Monitoring of Soil Nitrogen and Developing the Nonequilibrium Model to Compensate NH_4^+ Adsorption Impact. The long-term continuous performance of HS-ISM sensors was assessed in the real-world soil (Table S1). During the 14 day continuous test period, the NO_3^- HS-ISM sensors successfully captured two NO_3^- shocks (4.5−12.4 mg/L and 1.9−18.9 mg/L, orange lines in Figure 4a) on the ~second day and eighth day. The accuracy was examined by comparing with the lab-based validation results (orange hollow dots in Figure 4a). The

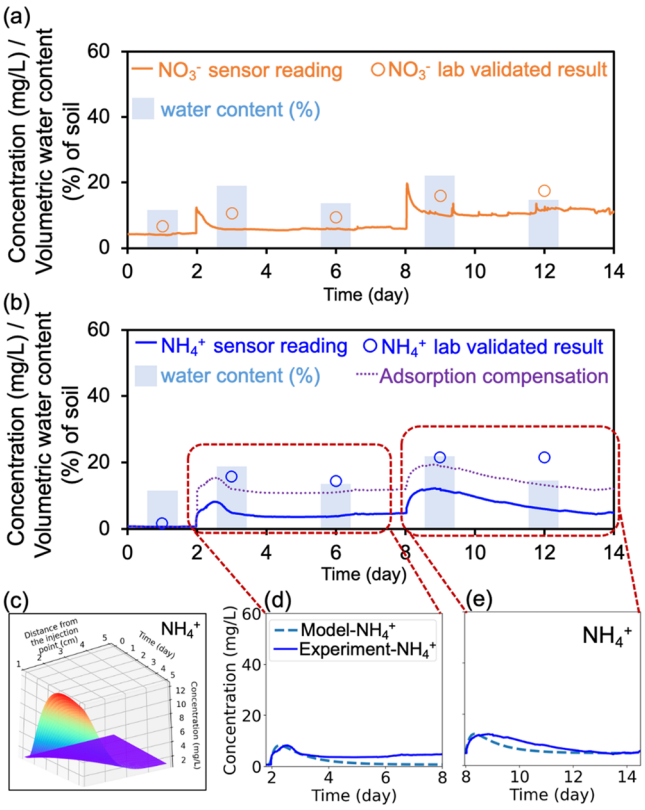

Figure 4. (a) Long-term real-time continuous readings (mg/L) of NO_3^- HS-ISM sensors (orange line) in soil over 14 days, comparison with the lab test result (orange dots) and corresponding volumetric water content (%) of soil (light blue column). (b) Long-term real-time continuous readings (mg/L) of NH_4^+ HS-ISM sensors (blue line) in soil over 14 days, comparison with the lab test result (blue dots), corresponding volumetric water content (%) of soil (light blue column), and adsorption compensated results (dotted lines). (c) 3D plot of the NH_4^+ transport process by integrating the chemical nonequilibrium NH_4^+ adsorption model. The fitted results of the NH_4^+ transport process at the depth 2 cm during the (d) 2−8 days and (e) 8−14 days.

discrepancy was less than 5 mg/L throughout the test period, which was evidently alleviated from the soil nitrate sensors reported previously, including nanofiber impedimetric nitrate soil sensors[59] (>10 mg/L), graphene/glassy carbon substrate soil nitrate electrodes[60] (>20 mg/L), and imprinted polymer-coated nitrate soil sensors[61] (>15 mg/L), indicating the high accuracy of the NO_3^- HS-ISM sensor in continuous monitoring. Additionally, after the volumetric water content (%, light blue columns in Figure 4a) of soil dropped to ~13% on the 6th and 12th day due to the water leaching and evaporation in the soil beaker, the HS-ISM NO_3^- sensor readings still sustained the good stability (discrepancy: ~5%, Figure 4a), demonstrating the distinct water-absorbent capability of the polyacrylamide hydrogel layer on the HS-ISM sensor that can maintain the ion equilibrium between the sensor surface and the S-ISM polymer matrix under low water content in soil. In contrast, the previous potentiometric soil sensor without a water-absorbent layer [e.g., polypyrrole PPy(NO_3^-)[9] and molybdenum disulfide (MoS_2)−poly(3-octyl-thiophene) soil sensors[10]] always suffered from the severe reading declination (sensor potential ≈ 0 mV) when soil water content (%) dropped below 15%. Furthermore, the hydrogel layer still maintained its intactness

https://doi.org/10.1021/acs.est.1c05661
Environ. Sci. Technol. XXXX, XXX, XXX−XXX

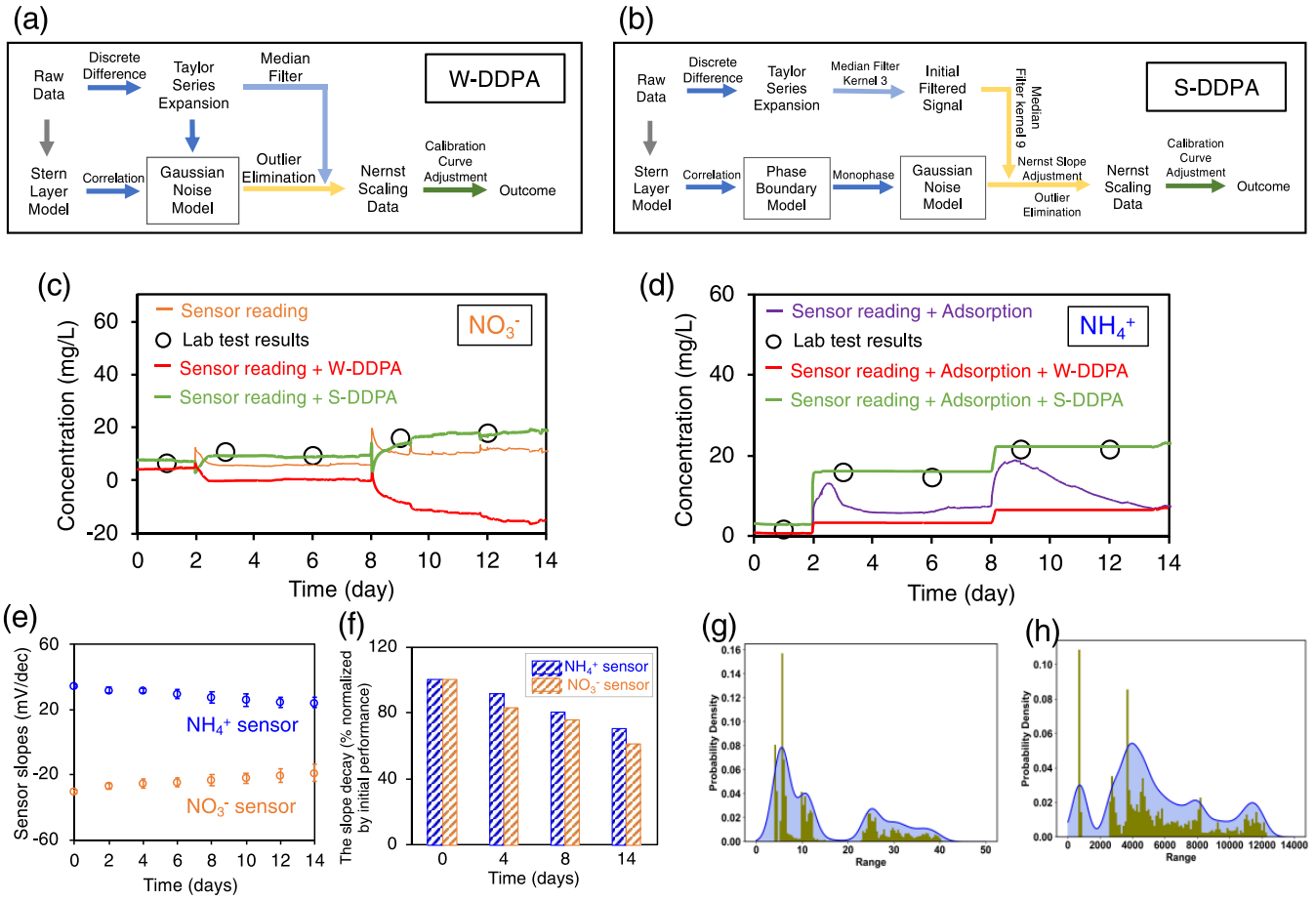

Figure 5. Flow chart of (a) W-DDPA and (b) S-DDPA processes. Comparison of processed data using W-DDPA and S-DDPA and sensor reading and lab test results for (c) NO_3^- and (d) NH_4^+ HS-ISM soil sensors. (e) Comparison of Nernst slopes between NO_3^- and NH_4^+ HS-ISM soil sensors over 14 days. (f) Nernst slope decay (%, normalized by the initial performance) of NO_3^- and NH_4^+ HS-ISM soil sensors over 14 days. (g) Original and process data distribution of the NO_3^- sensor. (h) Original and process data distribution of the NH_4^+ sensor.

after 15 day continuous insertion in soil, though high amounts of soil particles were attached to the sensor surface (Figure S6).

The OCP readings of the NH_4^+ HS-ISM soil sensor (blue lines in Figure 4b) patently displayed a larger discrepancy (~12 mg/L) than those of the NO_3^- HS-ISM sensors during the same test period, which mainly resulted from the NH_4^+ adsorption on soil particles. To validate this assumption, a nonequilibrium adsorption model was incorporated into the NH_4^+ transport model to fit the NH_4^+ sensor readings. In this model, the NH_4^+ adsorption rate was evitable at the beginning stage after two ammonium shocks were introduced on 2−3 and 8−9 days, respectively, and thereafter, the adsorption rate subsided to zero over time (3−8 and 9−14 days, eq 1). Additionally, various parameters (e.g., K, θ_e, S_e, and Ψ) in this model are dependent on the specific soil type (e.g., fine sandy loam soil) selected in this study (eq 3 and Table S2). These parameters were together considered into the determination of seepage velocity and then incorporated into the transport process to adjust this model (Text S5). Finally, based on the fitted average partition coefficient of $0.6e^{-0.02t}$, our modified NH_4^+ transport model (eqs 1−3) exhibited an excellent correlation with the NH_4^+ sensor readings (R^2 > 0.7, Figure 4c−e). Comparatively, the classic equilibrium transport model[38] failed to fit our sensor readings (R^2 < 0.5, Figure S7), since the equilibrium NH_4^+ adsorption in this model underestimated the change of the adsorption rate with time and assumed that the entire transport process sustained the same adsorption rate.[62] This result explicitly demonstrated the reliability of our nonequilibrium model in terms of quantifying the NH_4^+ adsorption capacity, and thus, we were able to reversely compensate the adsorption capacity (weights: $0.6e^{-0.02t}$) into the NH_4^+ sensor readings. The compensated NH_4^+ sensor readings successfully minimized the deviations from ~12 to ~4.8 mg/L (dotted line in Figure 4b), which highly enhanced the accuracy of NH_4^+ real-time monitoring in the soil environment. This NH_4^+ HS-ISM sensor with adsorption compensation (discrepancy: ~4.8 mg/L) has appreciably outperformed previous soil NH_4^+ sensors (e.g., laser-induced graphene sensor,[63] methylene Blue-modified sensors[64]).

3.4. Enhancing Accuracy of Long-Term Continuous Monitoring in the Soil Environment Using the Soil-Based Denoising Data Processing Algorithm (S-DDPA). Along with the nonlinear adsorption model (eqs 1−3) to reduce the sensor reading deviation for long-term continuous monitoring, a soil-based DDPA (S-DDPA) (eqs 4−6) was developed to further enhance the accuracy of soil sensors by differentiating and minimizing the residual discrepancies (~5 mg/L for NO_3^-, and ~4.8 mg/L for NH_4^+, Figure 4a,b) of HS-ISM sensors. In the water-based DDPA (W-DDPA) previously developed,[32] the interface was mainly divided into two layers: stern layer (static electricity and potential control layer) and inner diffusion layer (mass transfer layer) (Figure 5a). The ion movements in the

https://doi.org/10.1021/acs.est.1c05661
Environ. Sci. Technol. XXXX, XXX, XXX−XXX

diffusion layer were regarded as Brownian motion and could be statistically described as Gaussian math model, which was well adopted in the water environment to represent the average system state (Figure 5a). Nevertheless, the hydrogel layer of soil sensors impaired the direct contact of the sensors with the sensing environment (soil). Hence, the ordinary Gaussian model cannot be used to describe the ion diffusion process on the sensor−soil interface, and the potential energy generated from the concentration gradient was also not sufficient to break the energy barrier (Figure 5b). Additionally, the soil porosity and texture could cause large amounts of uninterpretable ion transport events and sensor reading noises.[65,66] Thereby, the conventional median filter and Taylor series expansion in the W-DDPA failed at recognizing these noises for the soil sensors (noise > 5 mg/L, red line in Figure 5c,d).

The S-DDPA doubled the median filter (eq 6) and incorporated the periodical variation of the Nernst slopes (mV/dec) into eqs 4−6 (e.g., the Nernst slopes of NO_3^- sensors and NH_4^+ sensors dropped from ∼30.5 to ∼18.5 mV/dec and from ∼35 to 24 mV/dec, respectively, Figure 5e,f). The double median filter could isolate nonlinear ion transfer in the hydrogel from the raw signal, differentiate the noise, and minimize the sensor reading drifting using the dynamically adjusted Nernst slopes (Figure 5b). The density analysis of the S-DDPA successfully calculated the distribution of the sensor OCP signals (mV) and the kernel density estimation (KDE) visualized two large bell-shaped peaks (Figure 5g,h) in the density histogram of the OCP data, indicating the corresponding two concentration gradients (shocks). Furthermore, we also upgraded the noise recognition capability in the S-DDPA (eq 4) by enclosing the hydrogel diffusion math model and Langmuir isotherms into the Taylor series expansion to balance the ion transport variations and hydrogel diffusion in the soil−hydrogel−sensor system. In this way, the parameters in the median filter and Taylor Series were corrected, and thus, the noise and drifting data outside the peaks can be discarded to stabilize the final data output. Namely, the separation of sensor signals was the identification of different processes (e.g., ion selectivity, Brownian motion, hydrogel diffusion, and soil water extraction) near the sensor surface, and the actual electrochemical response was compensated by minimizing the signal-to-noise ratio (SNR).[32] Compared with lab-based validation results without noises, the S-DDPA processed data (green line in Figure 5c,d) successfully minimized the data discrepancy (deviation) of the NO_3^- and NH_4^+ sensor readings from ∼5 and ∼4.8 to ∼1.9 and ∼1.5 mg/L (Figure 5c,d), respectively, satisfying the error requirement of commercial monitoring (<2 mg/L). To sum up, the S-DDPA as a novel algorithm fundamentally solved the problems encountered by the soil sensors, enabled dissecting the soil sensors' readings, removed background noise, and advanced the sensors' accuracy in the complex soil environment.

3.5. Challenges, Outlooks, and Future Studies. We have demonstrated that casting a thin layer of the water-absorbent polyacrylamide hydrogel onto solid-state sensors could comprehensively enhance the performance of HS-ISM nitrogen sensors in soil. Coupled with S-DDPA to further remove sensor reading noise, this sensor-algorithm platform offers the real-time, continuous, and long-term monitoring of dynamic nitrogen transport and fate in soil. Monitoring the spatial and temporal variability of soil nitrogen dynamics is capable of calibrating, validating, and improving parameterizations of the nitrogen biogeochemical cycles, thus addressing previous modeling uncertainties caused by the sparsity and inconsistence of soil nitrogen data. The improved model will also facilitate accurate real-time forecast of environmental quality and agricultural practice (e.g., fertilization and irrigation) and contribute to swift and effective decision making related to environmental protection and precision agriculture.

However, as an *in situ* technology, the biggest obstacle of HS-ISM sensors is the unknown external impact factors including soil biological properties (e.g., enzyme, pathogens, and microbial biomass) and drastic fluctuation of soil moisture contents that inevitably change the adjacent environment of the sensor surface, interfere ion and electron transfer between soil and sensor matrix, and ultimately impair the sensor electrochemical response. Further studies focusing on the kinetics of soil biological properties and HS-ISM soil sensor interaction models should be conducted to modulate and incorporate with S-DDPA and further elevate its correction capability for long-term continuous soil dynamic monitoring.

■ ASSOCIATED CONTENT

Supporting Information

The Supporting Information is available free of charge at https://pubs.acs.org/doi/10.1021/acs.est.1c05661.

Ultrathin layer of water-absorbent polyacrylamide hydrogel-coated solid-state ion-selective membrane (HS-ISM) sensors coupled with soil-based denoising data processing algorithm (S-DDPA) was developed to achieve real-time, *in situ*, continuous, and long-term monitoring of nitrogen transport and fate in soil; this innovative technology bears profound significance for a broad spectrum of soil-associated activities, such as soil system resilience, nutrient management, contaminant removal, and energy-saving practices6 (PDF)

Diagram of the experimental setup; details of the electrospray procedure for ISM; thickness measurement of the polyacrylamide hydrogel layer; lab validation of soil nitrogen concentration, and the brief description of calibration and selectivity measurement for HS-ISM sensors; details of the ammonium transport model development; the SEM and EDS images of the hydrogel and ISM surface; the structure of polyacrylamide hydrogel; the fitting results of the classic equilibrium model; soil parameters of the UConn Research Farm; and comparisons of diffusion and permeability coefficient with different hydrogel thicknesses based on eqs 5 and 6 (PDF)

■ AUTHOR INFORMATION

Corresponding Author

Baikun Li − *Department of Civil and Environmental Engineering, University of Connecticut, Storrs, Connecticut 06269, United States; Center for Environmental Science and Engineering, University of Connecticut, Storrs, Connecticut 06269, United States;* orcid.org/0000-0002-5623-5912; Phone: 860-486-2339; Email: baikun.li@uconn.edu

Authors

Yingzheng Fan − *Department of Civil and Environmental Engineering, University of Connecticut, Storrs, Connecticut 06269, United States*

https://doi.org/10.1021/acs.est.1c05661
Environ. Sci. Technol. XXXX, XXX, XXX−XXX

Xingyu Wang − *Department of Civil and Environmental Engineering, University of Connecticut, Storrs, Connecticut 06269, United States*
Xin Qian − *Department of Chemical and Biomolecular Engineering, University of Connecticut, Storrs, Connecticut 06269, United States;* orcid.org/0000-0001-8904-2802
Anand Dixit − *Institute of Materials Science, University of Connecticut, Storrs, Connecticut 06269, United States*
Brianna Herman − *Department of Civil and Environmental Engineering, University of Connecticut, Storrs, Connecticut 06269, United States*
Yu Lei − *Department of Chemical and Biomolecular Engineering, University of Connecticut, Storrs, Connecticut 06269, United States;* orcid.org/0000-0002-0184-0373
Jeffrey McCutcheon − *Department of Chemical and Biomolecular Engineering, University of Connecticut, Storrs, Connecticut 06269, United States*

Complete contact information is available at: https://pubs.acs.org/10.1021/acs.est.1c05661

Notes

The authors declare no competing financial interest.

■ ACKNOWLEDGMENTS

This study was supported by National Science Foundation (NSF) Environmental Engineering Program GOALI Project (Grant No.: 1706343), NSF Signal in the soil (SitS) Project (Grant No: 1935599), NSF Civil, Mechanical and Manufacturing Innovation (CMMI) Project (Grant No.: 2001544), and Connecticut SPARK Program. Some experiments are supported by Infiltrator Water Technologies Co.

■ REFERENCES

(1) Singh, S.; Bakshi, B. R. Accounting for the Biogeochemical Cycle of Nitrogen in Input-Output Life Cycle Assessment. *Environ. Sci. Technol.* **2013**, *47*, 9388−9396.
(2) Bukata, A. R.; Kyser, T. K. Carbon and Nitrogen Isotope Variations in Tree-Rings as Records of Perturbations in Regional Carbon and Nitrogen Cycles. *Environ. Sci. Technol.* **2007**, *41*, 1331−1338.
(3) Mia, S.; Dijkstra, F. A.; Singh, B. Aging Induced Changes in Biochar's Functionality and Adsorption Behavior for Phosphate and Ammonium. *Environ. Sci. Technol.* **2017**, *51*, 8359−8367.
(4) Gao, J.; Wang, S.; Li, Z.; Wang, L.; Chen, Z.; Zhou, J. High Nitrate Accumulation in the Vadose Zone after Land-Use Change from Croplands to Orchards. *Environ. Sci. Technol.* **2021**, *55*, 5782−5790.
(5) Rogovska, N.; Laird, D. A.; Chiou, C. P.; Bond, L. J. Development of Field Mobile Soil Nitrate Sensor Technology to Facilitate Precision Fertilizer Management. *Precis. Agric.* **2019**, *20*, 40−55.
(6) Hu, J.; Stein, A.; Bühlmann, P. Rational Design of All-Solid-State Ion-Selective Electrodes and Reference Electrodes. *TrAC, Trends Anal. Chem.* **2016**, *76*, 102−114.
(7) Athavale, R.; Kokorite, I.; Dinkel, C.; Bakker, E.; Wehrli, B.; Crespo, G. A.; Brand, A. In Situ Ammonium Profiling Using Solid-Contact Ion-Selective Electrodes in Eutrophic Lakes. *Anal. Chem.* **2015**, *87*, 11990−11997.
(8) Fan, Y.; Huang, Y.; Linthicum, W.; Liu, F.; Beringhs, A. O.; Dang, Y.; Xu, Z.; Chang, S.-Y.; Ling, J.; Huey, B. D. Toward Long-Term Accurate and Continuous Monitoring of Nitrate in Wastewater Using Poly (Tetrafluoroethylene)(PTFE)−Solid-State Ion-Selective Electrodes (S-ISEs). *ACS Sens.* **2020**, *5*, 3182−3193.
(9) Chen, M.; Zhang, M.; Wang, X.; Yang, Q.; Wang, M.; Liu, G.; Yao, L. An All-Solid-State Nitrate Ion-Selective Electrode with Nanohybrids Composite Films for In-Situ Soil Nutrient Monitoring. *Sensors* **2020**, *20*, No. 2270.
(10) Ali, M. A.; Wang, X.; Chen, Y.; Jiao, Y.; Mahal, N. K.; Moru, S.; Castellano, M. J.; Schnable, J. C.; Schnable, P. S.; Dong, L. Continuous Monitoring of Soil Nitrate Using a Miniature Sensor with Poly(3-Octyl-Thiophene) and Molybdenum Disulfide Nanocomposite. *ACS Appl. Mater. Interfaces* **2019**, *11*, 29195−29206.
(11) Fan, Y.; Xu, Z.; Huang, Y.; Wang, T.; Zheng, S.; DePasquale, A.; Brüeckner, C.; Lei, Y.; Li, B. Long-Term Continuous and Real-Time in Situ Monitoring of Pb(II) Toxic Contaminants in Wastewater Using Solid-State Ion Selective Membrane (S-ISM) Pb and PH Auto-Correction Assembly. *J. Hazard. Mater.* **2020**, *400*, No. 123299.
(12) Futagawa, M.; Ito, T.; Kunii, A.; Watanabe, M.; Suzuki, H.; Fuwa, Y.; Takeshita, Y.; Komatsu, M. In *Fabrication of a Hydrophilic Property Impedance Sensor to Stably Monitor Soil Water Content for Slope Failure Prognostics*, 2015 IEEE Sensors; IEEE, 2015; pp 1−4.
(13) Chen, Y.; Tian, Y.; Wang, X.; Dong, L. In *Miniaturized Soil Sensor for Continuous, in-Situ Monitoring of Soil Water Potential*, 2019 20th International Conference on Solid-State Sensors, Actuators and Microsystems & Eurosensors XXXIII (TRANSDUCERS & EUROSENSORS XXXIII); IEEE, 2019; pp 2025−2028.
(14) Laftah, W. A.; Hashim, S.; Ibrahim, A. N. Polymer Hydrogels: A Review. *Polym.-Plast. Technol. Eng.* **2011**, *50*, 1475−1486.
(15) Zolfaghari, R.; Katbab, A. A.; Nabavizadeh, J.; Tabasi, R. Y.; Nejad, M. H. Preparation and Characterization of Nanocomposite Hydrogels Based on Polyacrylamide for Enhanced Oil Recovery Applications. *J. Appl. Polym. Sci.* **2006**, *100*, 2096−2103.
(16) Ali, M. A. M.; Alsabagh, A. M.; Sabaa, M. W.; El-Salamony, R. A.; Mohamed, R. R.; Morsi, R. E. Polyacrylamide Hybrid Nanocomposites Hydrogels for Efficient Water Treatment. *Iran. Polym. J.* **2020**, *29*, 455−466.
(17) Ono, S.; Ogawa, R.; Hyakusoku, H. Complications after Polyacrylamide Hydrogel Injection for Soft-Tissue Augmentation. *Plast. Reconstr. Surg.* **2010**, *126*, 1349−1357.
(18) Ge, G.; Zhang, Y.; Shao, J.; Wang, W.; Si, W.; Huang, W.; Dong, X. Stretchable, Transparent, and Self-Patterned Hydrogel-Based Pressure Sensor for Human Motions Detection. *Adv. Funct. Mater.* **2018**, *28*, No. 1802576.
(19) Chen, C.; Dong, Z.-Q.; Shen, J.-H.; Chen, H.-W.; Zhu, Y.-H.; Zhu, Z.-G. 2D Photonic Crystal Hydrogel Sensor for Tear Glucose Monitoring. *ACS Omega* **2018**, *3*, 3211−3217.
(20) Rizvi, A. S.; Murtaza, G.; Yan, D.; Irfan, M.; Xue, M.; Meng, Z. H.; Qu, F. Development of Molecularly Imprinted 2D Photonic Crystal Hydrogel Sensor for Detection of L-Kynurenine in Human Serum. *Talanta* **2020**, *208*, No. 120403.
(21) Yuk, H.; Zhang, T.; Lin, S.; Parada, G. A.; Zhao, X. Tough Bonding of Hydrogels to Diverse Non-Porous Surfaces. *Nat. Mater.* **2016**, *15*, 190−196.
(22) Wancura, M.; Talanker, M.; Toubbeh, S.; Bryan, A.; Cosgriff-Hernandez, E. Bioactive Hydrogel Coatings of Complex Substrates Using Diffusion-Mediated Redox Initiation. *J. Mater. Chem. B* **2020**, *8*, 4289−4298.
(23) Yao, X.; Liu, J.; Yang, C.; Yang, X.; Wei, J.; Xia, Y.; Gong, X.; Suo, Z. Hydrogel Paint. *Adv. Mater.* **2019**, *31*, No. 1903062.
(24) Suárez, F.; Bachmann, J.; Muñoz, J. F.; Ortiz, C.; Tyler, S. W.; Alister, C.; Kogan, M. Transport of Simazine in Unsaturated Sandy Soil and Predictions of Its Leaching under Hypothetical Field Conditions. *J. Contam. Hydrol.* **2007**, *94*, 166−177.
(25) Ardakani, M. S.; McLaren, A. D. Absence of Local Equilibrium during Ammonium Transport in a Soil Column. *Soil Sci. Soc. Am. J.* **1977**, *41*, 877−879.
(26) Jellali, S.; Diamantopoulos, E.; Kallali, H.; Bennaceur, S.; Anane, M.; Jedidi, N. Dynamic Sorption of Ammonium by Sandy Soil in Fixed Bed Columns: Evaluation of Equilibrium and Non-Equilibrium Transport Processes. *J. Environ. Manage.* **2010**, *91*, 897−905.
(27) Griffin, G.; Jokela, W.; Ross, D.; Pettinelli, D.; Morris, T.; Wilf, A. Recommended Soil Nitrate-N Tests. In *Recommended Soil Testing Procedures for the Northeastern United States*; Northeastern Regional Publication No. 493, 1995.
(28) Elghobashy, M. R.; Mahmoud, A. M.; Rezk, M. R.; El-Rahman, M. K. A. Strategy for Fabrication of Stable Tramadol Solid-Contact Ion-

Selective Potentiometric Sensor Based on Polyaniline Nanoparticles. *J. Electrochem. Soc.* **2015**, *162*, No. H1.
(29) Liakos, K. G.; Busato, P.; Moshou, D.; Pearson, S.; Bochtis, D. Machine Learning in Agriculture: A Review. *Sensors* **2018**, *18*, No. 2674.
(30) Behrens, T.; Zhu, A.-X.; Schmidt, K.; Scholten, T. Multi-Scale Digital Terrain Analysis and Feature Selection for Digital Soil Mapping. *Geoderma* **2010**, *155*, 175−185.
(31) Vergara, A.; Vembu, S.; Ayhan, T.; Ryan, M. A.; Homer, M. L.; Huerta, R. Chemical Gas Sensor Drift Compensation Using Classifier Ensembles. *Sens. Actuators, B* **2012**, *166−167*, 320−329.
(32) Wang, X.; Fan, Y.; Huang, Y.; Ling, J.; Klimowicz, A.; Pagano, G.; Li, B. Solving Sensor Reading Drifting Using Denoising Data Processing Algorithm (DDPA) for Long-Term Continuous and Accurate Monitoring of Ammonium in Wastewater. *ACS EST Water* **2021**, *1*, 530−541.
(33) Huang, Y.; Wang, T.; Xu, Z.; Hughes, E.; Qian, F.; Lee, M.; Fan, Y.; Lei, Y.; Brückner, C.; Li, B. Real-Time in Situ Monitoring of Nitrogen Dynamics in Wastewater Treatment Processes Using Wireless, Solid-State, and Ion-Selective Membrane Sensors. *Environ. Sci. Technol.* **2019**, *53*, 3140−3148.
(34) Fan, Y.; Qian, X.; Wang, X.; Funk, T.; Herman, B.; McCutcheon, J. R.; Li, B. Enhancing Long-Term Accuracy and Durability of Wastewater Monitoring Using Electrosprayed Ultra-Thin Solid-State Ion Selective Membrane Sensors. *J. Membr. Sci.* **2022**, *643*, No. 119997.
(35) Liao, I. C.; Moutos, F. T.; Estes, B. T.; Zhao, X.; Guilak, F. Composite Three-Dimensional Woven Scaffolds with Interpenetrating Network Hydrogels to Create Functional Synthetic Articular Cartilage. *Adv. Funct. Mater.* **2013**, *23*, 5833−5839.
(36) Benoit, R.; Wilkinson, K. J.; Sauvé, S. Partitioning of Silver and Chemical Speciation of Free Ag in Soils Amended with Nanoparticles. *Chem. Cent. J.* **2013**, *7*, No. 75.
(37) Knox, R. C.; Sabatini, D. A.; Canter, L. W. *Subsurface Transport and Fate Processes*; CRC Press: Boca Raton, 2017.
(38) Hemond, H. F.; Fechner, E. J. *Chemical Fate and Transport in the Environment*; Elsevier, 2014.
(39) White, M. L. The Permeability of an Acrylamide Polymer Gel. *J. Phys. Chem. A* **1960**, *64*, 1563−1565.
(40) Hoch, G.; Chauhan, A.; Radke, C. J. Permeability and Diffusivity for Water Transport through Hydrogel Membranes. *J. Membr. Sci.* **2003**, *214*, 199−209.
(41) Zhao, B.; Ma, W.; Zhang, P.; Zhang, Q.; Zhong, J.; Matsuyama, H. Permeation and Diffusion of Nutrient Ions in Poly (Vinyl Alcohol) Hydrogel Membrane. *Chem. Pap.* **2020**, *74*, 3913−3923.
(42) Wu, Y.; Joseph, S.; Aluru, N. R. Effect of Cross-Linking on the Diffusion of Water, Ions, and Small Molecules in Hydrogels. *J. Phys. Chem. B* **2009**, 3512−3520.
(43) Amsden, B. Modeling Solute Diffusion in Aqueous Polymer Solutions. *Polymer* **2002**, *43*, 1623−1630.
(44) Weber, L. M.; Lopez, C. G.; Anseth, K. S. Effects of PEG Hydrogel Crosslinking Density on Protein Diffusion and Encapsulated Islet Survival and Function. *J. Biomed. Mater. Res., Part A* **2009**, *90*, 720−729.
(45) Kanmaz, N.; Saloglu, D.; Hizal, J. Humic Acid Embedded Chitosan/Poly (Vinyl Alcohol) PH-Sensitive Hydrogel: Synthesis, Characterization, Swelling Kinetic and Diffusion Coefficient. *Chem. Eng. Commun.* **2019**, *206*, 1168−1180.
(46) Horneck, D. A.; Sullivan, D. M.; Owen, J. S.; Hart, J. M. *Soil Test Interpretation Guide*; Oregon State University Extension Service, 2011.
(47) Alva, S.; Sundari, R.; A Aziz, A. S.; A Rashid, N. A.; Gunawan, W. Development of Ammonium-Selective Electrode Based on PVC/MB28 Membrane. In *IOP Conference Series: Materials Science and Engineering*; IOP Publishing, 2018; Vol. *453*, p 012042.
(48) Kan, Y. An All-Solid-State Ammonium Ion-Selective Electrode Based on Polyaniline as Transducer and Poly (o-Phenylenediamine) as Sensitive Membrane. *Int. J. Electrochem. Sci.* **2016**, 9928−9940.
(49) Minami, T.; Sasaki, Y.; Minamiki, T.; Wakida, S.; Kurita, R.; Niwa, O.; Tokito, S. Selective Nitrate Detection by an Enzymatic Sensor Based on an Extended-Gate Type Organic Field-Effect Transistor. *Biosens. Bioelectron.* **2016**, *81*, 87−91.
(50) Mahmoudian, M. R.; Alias, Y.; Basirun, W. J.; MengWoi, P.; Jamali-Sheini, F.; Sookhakian, M.; Silakhori, M. A Sensitive Electrochemical Nitrate Sensor Based on Polypyrrole Coated Palladium Nanoclusters. *J. Electroanal. Chem.* **2015**, *751*, 30−36.
(51) Chin, J.; Oh, J.; Jon, S. Y.; Park, S. H.; Walsdorff, C.; Stranix, B.; Ghoussoub, A.; Lee, S. J.; Chung, H. J.; Park, S.-M.; Kim, K. Tuning and Dissecting Electronic and Steric Effects in Ammonium Receptors: Nonactin vs Artificial Receptors. *J. Am. Chem. Soc.* **2002**, *124*, 5374−5379.
(52) Singh, A. S.; Sun, S.-S. Recognition, Encapsulation, and Selective Fluorescence Sensing of Nitrate Anion by Neutral C3-Symmetric Tripodal Podands Bearing Amide Functionality. *J. Org. Chem.* **2012**, *77*, 1880−1890.
(53) Hurraß, J.; Schaumann, G. E. Properties of Soil Organic Matter and Aqueous Extracts of Actually Water Repellent and Wettable Soil Samples. *Geoderma* **2006**, *132*, 222−239.
(54) Kusel, K.; Drake, H. L. Effects of Environmental Parameters on the Formation and Turnover of Acetate by Forest Soils. *Appl. Environ. Microbiol.* **1995**, *61*, 3667−3675.
(55) Hendi, A.; Umair Hassan, M.; Elsherif, M.; Alqattan, B.; Park, S.; Yetisen, A. K.; Butt, H. Healthcare Applications of PH-Sensitive Hydrogel-Based Devices: A Review. *Int. J. Nanomed.* **2020**, *15*, 3887−3901.
(56) Jiang, H.; Yu, W.; Waimin, J. F.; Glassmaker, N.; Raghunathan, N.; Jiang, X.; Ziaie, B.; Rahimi, R. In *Inkjet-Printed Solid-State Potentiometric Nitrate Ion Selective Electrodes for Agricultural Application*, 2019 IEEE SENSORS; IEEE, 2019; pp 26−29.
(57) Liao, Y.-H.; Chou, J.-C. Preparation and Characteristics of Ruthenium Dioxide for PH Array Sensors with Real-Time Measurement System. *Sens. Actuators, B* **2008**, *128*, 603−612.
(58) Friedrich, J.; Altmann, K.; Wettmarshausen, S.; Hidde, G. Coating of Carbon Fibers with Adhesion-Promoting Thin Polymer Layers Using Plasma Polymerization or Electrospray Ionization Technique—A Comparison. *Plasma Process. Polym.* **2017**, *14*, No. 1600074.
(59) Ali, M. A.; Jiang, H.; Mahal, N. K.; Weber, R. J.; Kumar, R.; Castellano, M. J.; Dong, L. Microfluidic Impedimetric Sensor for Soil Nitrate Detection Using Graphene Oxide and Conductive Nanofibers Enabled Sensing Interface. *Sens. Actuators, B* **2017**, *239*, 1289−1299.
(60) Pan, P.; Miao, Z.; Yanhua, L.; Linan, Z.; Haiyan, R.; Pan, K.; Linpei, P.; et al. Preparation and Evaluation of a Stable Solid State Ion Selective Electrode of Polypyrrole/Electrochemically Reduced Graphene/Glassy Carbon Substrate for Soil Nitrate Sensing. *Int. J. Electrochem. Sci.* **2016**, *11*, 4779−4793.
(61) Alahi, M. E. E.; Mukhopadhyay, S. C.; Burkitt, L. Imprinted Polymer Coated Impedimetric Nitrate Sensor for Real- Time Water Quality Monitoring. *Sens. Actuators, B* **2018**, *259*, 753−761.
(62) Selim, H. M. *Transport & Fate of Chemicals in Soils: Principles & Applications*; CRC Press, 2014.
(63) Garland, N. T.; McLamore, E. S.; Cavallaro, N. D.; Mendivelso-Perez, D.; Smith, E. A.; Jing, D.; Claussen, J. C. Flexible Laser-Induced Graphene for Nitrogen Sensing in Soil. *ACS Appl. Mater. Interfaces* **2018**, *10*, 39124−39133.
(64) Keskin, B.; Üzer, A.; Apak, R. Colorimetric Sensing of Ammonium Perchlorate Using Methylene Blue- Modified Gold Nanoparticles. *Talanta* **2020**, *206*, No. 120240.
(65) Liu, G.; Xue, W.; Wang, J.; Liu, X. Transport Behavior of Variable Charge Soil Particle Size Fractions and Their Influence on Cadmium Transport in Saturated Porous Media. *Geoderma* **2019**, *337*, 945−955.
(66) Ray, N.; Rupp, A.; Schulz, R.; Knabner, P. Old and New Approaches Predicting the Diffusion in Porous Media. *Transp. Porous Media* **2018**, *124*, 803−824.

https://doi.org/10.1021/acs.est.1c05661
Environ. Sci. Technol. XXXX, XXX, XXX−XXX